


## Complete Frequency-Bin Bell Basis Synthesizer

Suparna Seshadri<sup>1</sup>, Hsuan-Hao Lu<sup>2</sup>, Daniel E. Leaird<sup>1</sup>, Andrew M. Weiner<sup>1</sup>, and Joseph M. Lukens<sup>2,3,\*</sup>

<sup>1</sup>*Elmore Family School of Electrical and Computer Engineering and Purdue Quantum Science and Engineering Institute, Purdue University, West Lafayette, Indiana 47907, USA*

<sup>2</sup>*Quantum Information Science Section, Oak Ridge National Laboratory, Oak Ridge, Tennessee 37831, USA*

<sup>3</sup>*Research Technology Office, Arizona State University, Tempe, Arizona 85287, USA*

 (Received 11 May 2022; revised 8 August 2022; accepted 27 October 2022; published 2 December 2022)

We report the experimental generation of all four frequency-bin Bell states in a single versatile setup via successive pumping of spontaneous parametric down-conversion with single and dual spectral lines. Our scheme utilizes intensity modulation to control the pump configuration and offers turn-key generation of any desired Bell state using only off-the-shelf telecommunication equipment. We employ Bayesian inference to reconstruct the density matrices of the generated Bell states, finding fidelities  $\geq 97\%$  for all cases. Additionally, we demonstrate the sensitivity of the frequency-bin Bell states to common-mode and differential-mode temporal delays traversed by the photons comprising the state—presenting the potential for either enhanced resolution or nonlocal sensing enabled by our complete Bell basis synthesizer.

DOI: [10.1103/PhysRevLett.129.230505](https://doi.org/10.1103/PhysRevLett.129.230505)

**Introduction.**—Bell states are vital resources both for fundamental investigations of quantum entanglement and for realizing practical goals in quantum information processing and metrology. Generation and measurement of Bell states appear in a plethora of quantum communication protocols spanning dense coding [1], teleportation [2], cryptography [3–5], and entanglement swapping [6,7]. Production of a complete set of Bell states has been actively studied in various photonic encodings including polarization [1,8], orbital angular momentum [9], time bins [10,11], and path [12–14]. Recently, interest in time-frequency encodings in general [15–19]—and frequency-bin encoding in particular [20–24]—has grown due to its multiplexing capabilities and compatibility with both on-chip integration and optical fiber networks. In frequency bins, the *negative* correlations associated with the  $|\Psi^\pm\rangle \propto |01\rangle \pm |10\rangle$  Bell states (under the convention where the logical  $|1\rangle$  has higher frequency than logical  $|0\rangle$  for each photon) are automatically realized through energy conservation in a nonlinear parametric process driven by a continuous-wave (cw) monochromatic pump. However, the generation of *positively* frequency-correlated  $|\Phi^\pm\rangle \propto |00\rangle \pm |11\rangle$  states is inherently more challenging. While the  $|\Psi^\pm\rangle$  states can be deterministically transformed to  $|\Phi^\pm\rangle$  states using a quantum frequency processor (QFP) [25], such transformations require multiple active elements after photon generation, increasing complexity and insertion losses.

In this Letter we synthesize all four frequency-bin Bell states in a single setup. Just as the superposition of multiple generation pathways (spatial, temporal, or polarization) underpins the production of Bell states in traditional encodings, our approach leverages the coherent superposition of multiple pump lines to shift from  $|\Psi^\pm\rangle$  to the

positively correlated  $|\Phi^\pm\rangle$  in spontaneous parametric down-conversion (SPDC). We use Bayesian estimation to reconstruct the density matrices of the generated Bell states and find fidelities  $\geq 97\%$ . The presented scheme together with the recent demonstration of a frequency-bin Bell state analyzer [26] and arbitrary control of frequency-bin qubits [23] lays the groundwork for several entanglement-based quantum networking protocols. Our Letter also opens up avenues in quantum metrology. The generation of all four frequency-bin Bell states enables selective implementation of complementary quantum-enhanced delay sensing capabilities: nonlocal differential-mode delay measurements with  $|\Psi^\pm\rangle$  and a two-photon advantage in common-mode delays with  $|\Phi^\pm\rangle$ . We demonstrate the concept by probing the impacts of common-mode and differential-mode phases, highlighting the potential to sense the link latency or perform positioning and clock synchronization [27,28] in entanglement distribution networks.

**Background.**—Consider two frequency-bin qubits defined on a comb-like grid of narrow band spectral modes spaced by multiples of  $\Delta\omega$  [29]. An arbitrary pure two-photon state for an idler  $I$  and signal  $S$  qubit can then be expressed as

$$|\psi\rangle = \gamma_{00}|I_0S_0\rangle + \gamma_{01}|I_0S_1\rangle + \gamma_{10}|I_1S_0\rangle + \gamma_{11}|I_1S_1\rangle, \quad (1)$$

where  $I_n$  ( $S_n$ ) signifies a single photon populating mode centered at frequency  $\omega_{I,n} = \omega_{I,0} + n\Delta\omega$  ( $\omega_{S,n} = \omega_{S,0} + n\Delta\omega$ ). In exploring the feasibility of producing such a state through SPDC, we note immediately that three pump wavelengths will be required to satisfy energy conservation for the four logical states:  $\omega_{P,-1} = \omega_{I,0} + \omega_{S,0}$ ,  $\omega_{P,0} = \omega_{I,0} + \omega_{S,1} = \omega_{I,1} + \omega_{S,0}$ , and  $\omega_{P,1} = \omega_{I,1} + \omega_{S,1}$ . We

therefore can write the basis coefficients  $\gamma_{mn}$  in terms of complex pump amplitudes  $\alpha_k$  corresponding to pump frequency lines at  $\omega_{P,k}$  [30]:  $\gamma_{00} = \alpha_{-1}\beta_{00}$ ,  $\gamma_{01} = \alpha_0\beta_{01}$ ,  $\gamma_{10} = \alpha_0\beta_{10}$ , and  $\gamma_{11} = \alpha_1\beta_{11}$ , where  $\beta_{mn} \equiv \beta(\omega_{I,m}, \omega_{S,n})$  denotes the phase-matching coefficient.

Accordingly, with full control of three pump lines and the relevant phase-matching conditions, it is, in principle, possible to produce any two-qubit frequency-bin pure state. Yet despite a large body of research on engineered periodic poling designs for nonlinear crystals [31], which in the context of biphoton generation include chirped patterns for increased bandwidth [32–34], phase-modulated patterns for pump switching [35,36], and Gaussian patterns to remove spectral entanglement [37–39], we are unaware of any method to leverage such engineering for fully arbitrary control over the  $\beta_{mn}$  phase-matching factors, as would be required for general two-qubit frequency-bin states. Indeed, if seeking a single physical configuration to produce all states of interest, the condition  $|\beta_{00}| \approx |\beta_{01}| \approx |\beta_{10}| \approx |\beta_{11}|$  would actually prove desirable in enabling comparable efficiency for all logical basis states. Under this condition, direct production of an arbitrary state is no longer possible, for the dependence of both  $\gamma_{01}$  and  $\gamma_{10}$  on  $\alpha_0$  prevents independent specification of each coefficient [40]. Nevertheless, all four Bell states can be generated:  $\alpha_{\pm 1} = 0$  and  $\alpha_0 \neq 0$  leads to  $|\gamma_{00}| = |\gamma_{11}| = 0$  and  $|\gamma_{01}| = |\gamma_{10}| \neq 0$ , whereas  $|\alpha_1| = |\alpha_{-1}| \neq 0$  and  $\alpha_0 = 0$  yields  $|\gamma_{00}| = |\gamma_{11}| \neq 0$  and  $|\gamma_{01}| = |\gamma_{10}| = 0$ . By applying phase shifts using a pulse shaper after generation—which would likely be present already for subsequent routing and processing—the specific phases required for  $|\Psi^\pm\rangle$  and  $|\Phi^\pm\rangle$  can be realized. Importantly, since switching between  $|\Psi^\pm\rangle$  and  $|\Phi^\pm\rangle$  is effected by modifying the pump, the generated photons experience no additional loss in the process.

**Bell state demonstration.**—Figure 1(a) depicts our frequency-bin Bell basis synthesizer. A cw laser centered at 780.3 nm ( $\omega_{P,0}/2\pi = 384.15$  THz) is launched into an electro-optic intensity modulator (EOIM) driven by a 25 GHz radio-frequency (rf) sinusoidal waveform, set to one of two desired modes of operation: in the “EOIM off” case, the rf waveform is suppressed and the dc bias point adjusted for maximum transmission, resulting in a single pump line; in the “EOIM on” case, a rf waveform with a 3.6 V peak amplitude—approximately 70% of the EOIM’s half-wave voltage—is applied while the dc bias point is set to the null transmission point, leading to two spectral lines spaced at 50 GHz via carrier suppression. The output from the EOIM is used to pump a fiber-pigtailed periodically poled lithium niobate (PPLN) ridge waveguide engineered for type-0 phase matching and temperature tuned to  $\sim 56^\circ\text{C}$  for maximum efficiency at the pump frequency  $\omega_{P,0}$ . Two 14 GHz-wide frequency bins separated by  $\Delta\omega/2\pi = 25$  GHz are carved using a pulse shaper (Shaper 1) at spacings of  $\pm 152.5$  GHz (for  $I_1$  and  $S_0$ ) and  $\pm 177.5$  GHz (for  $I_0$  and  $S_1$ ) on either side of the cw laser’s half-frequency ( $\frac{1}{2}\omega_{P,0}$ ).

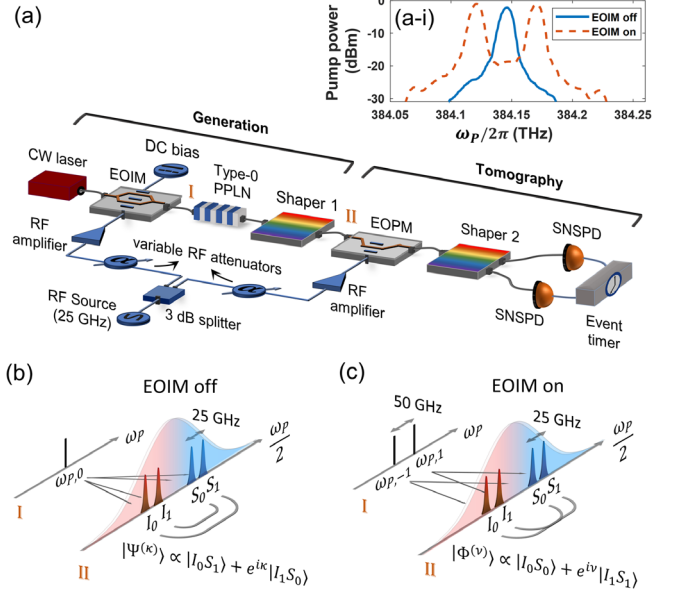


FIG. 1. (a) Experimental setup. Frequency domain illustration for the generation of (b)  $|\Psi^{(\kappa)}\rangle$ - and (c)  $|\Phi^{(\nu)}\rangle$ -type states. See text for details. (a-i) Measured pump spectra.

The produced state is then characterized by a tomography setup comprising an electro-optic phase modulator (EOPM), a pulse shaper operated as a wavelength-selective switch (Shaper 2), and two superconducting nanowire single-photon detectors (SNSPDs) for coincidence detection. When the EOPM drive signal is off, the measured joint spectral intensity (JSI) corresponds to application of the identity to both signal and idler photons ( $\mathbb{I}_I \otimes \mathbb{I}_S$ ); when the 25 GHz EOPM signal is on (with modulation index  $m = 1.435$  rad to ensure equal mixing probability between two adjacent bins), both photons experience a probabilistic Hadamard gate ( $\mathbb{H}_I \otimes \mathbb{H}_S$ ) [23,41] prior to spectrally resolved detection.

In the first experiment [Fig. 1(b)], we couple a single carrier pump ( $\omega_{P,0}$ ) at 6.2 mW into the PPLN waveguide. After spectral filtering, the resulting state is ideally of the form  $|\Psi^{(\kappa)}\rangle \propto |I_0S_1\rangle + e^{i\kappa}|I_1S_0\rangle$ , where the phase  $\kappa$  is dependent on the difference in delays experienced by the biphotons prior to the EOPM [42]. Since both photons traverse identical links with negligible dispersion,  $\kappa$  is expected to be zero. We verify the same by measuring the coincidences between all pairs of signal and idler frequency bins selected by Shaper 2 while the spectral phase on the bin pair  $|I_1S_0\rangle$  is scanned by Shaper 1 followed by parallel Hadamard gates applied by the EOPM. The phase  $\kappa$  is set to 0 ( $\pi$ ) using Shaper 1 to obtain the standard Bell state  $|\Psi^+\rangle \equiv |\Psi^{(0)}\rangle$  ( $|\Psi^-\rangle \equiv |\Psi^{(\pi)}\rangle$ ).

Figure 2(a) shows the measured coincidences after applying gate operations  $\mathbb{I}_I \otimes \mathbb{I}_S$  and  $\mathbb{H}_I \otimes \mathbb{H}_S$ —corresponding to measurement in the  $Z \otimes Z$  and  $X \otimes X$  Pauli bases, respectively. In accordance with theory [42], the negative frequency correlations revealed in the  $\mathbb{I}_I \otimes \mathbb{I}_S$  JSI

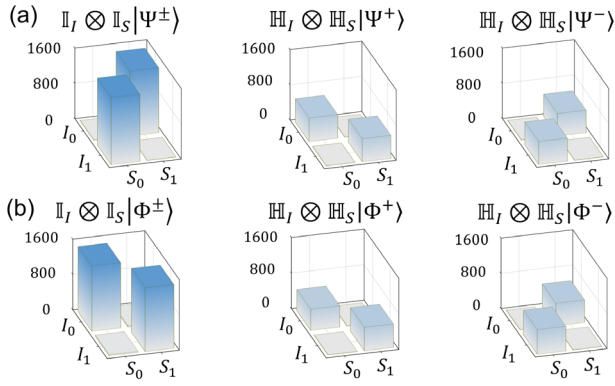


FIG. 2. Coincidences (integrated over 4 s) between output frequency bins after the operations  $\mathbb{I}_l \otimes \mathbb{I}_s$  and  $\mathbb{H}_l \otimes \mathbb{H}_s$  for (a)  $|\Psi^\pm\rangle$  and (b)  $|\Phi^\pm\rangle$ . The coincidence window is 256 ps.

are reversed after the Hadamards for the  $|\Psi^+\rangle$  Bell state, but retained for  $|\Psi^-\rangle$ . A factor of  $\sim 2.8$  lower coincidences for the  $\mathbb{H}_l \otimes \mathbb{H}_s$  cases result from the probabilistic nature of the single-EOPM Hadamard [41].

In the second experiment [Fig. 1(c)], the EOIM eliminates the original pump line at  $\omega_{P,0}$  and produces equal first-order sidebands spaced by 50 GHz ( $\omega_{P,-1}$  and  $\omega_{P,1}$ ). The power in each sideband after modulation is maintained at  $\sim 7$  mW in order to achieve coincidence rates similar to the first experiment. Note that this amounts to approximately twice the total pump power as before: in the spontaneous regime, the flux in any given signal-idler bin pair is directly proportional to the pump power at the corresponding sum frequency, so that the two pump lines in the EOIM on case must *each* match the power of the single line in the EOIM off case to maintain the rate of Bell state production. Experimentally, we observe 17.5 dB extinction of the original line [Fig. 1(a-i)], implying a roughly 50-fold suppression of negatively correlated biphoton contributions relative to the desired positive correlations. Such intensity modulation offers a particularly simple approach for producing the two lines required, although more general pump inputs would be possible with an optical frequency comb as input—e.g., an EOPM followed by a line-by-line pulse shaper in the 780 nm wavelength band [46,47]. Such an arrangement would allow for arbitrary weightings of the input pump lines, but introduce additional complexity that is not required for the Bell states of interest here.

The succeeding SPDC process generates time-energy entangled biphotons in coherent superpositions of broadband spectral amplitudes centered at half of the pump-sideband frequencies, resulting in a two-qubit entangled state ideally of the form  $|\Phi^{(\nu)}\rangle \propto |I_0 S_0\rangle + e^{i\nu} |I_1 S_1\rangle$ . The phase  $\nu$  is a fixed common-mode phase that is expected from the rf modulation phase and mean optical delay traversed by the biphotons [42]. We determine the phase  $\nu$  in the same fashion as with  $\kappa$  but now by scanning the spectral phase imparted on the bin pair  $|I_1 S_1\rangle$ ; the measured value of  $\nu$  is compensated for and set to 0 ( $\pi$ ) to obtain

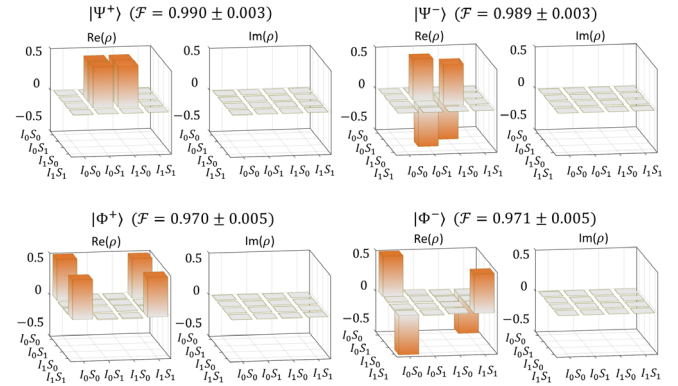


FIG. 3. Bayesian mean density matrices computed from the measurements in Fig. 2.

$|\Phi^+\rangle \equiv |\Phi^{(0)}\rangle$  ( $|\Phi^-\rangle \equiv |\Phi^{(\pi)}\rangle$ ). Measured JSIs after the identity and Hadamard operations appear in Fig. 2(b); in contrast to the  $|\Psi^\pm\rangle$  case, positive frequency correlations are now clearly evident in the  $\mathbb{I}_l \otimes \mathbb{I}_s$  measurement, with the Hadamard operation producing correlation patterns that depend on the state phase (0 or  $\pi$ ).

Figure 2 reveals unique correlation signatures for each state in the results from both identity and Hadamard. Such signatures are sufficient to perform high-fidelity state quantum reconstruction via Bayesian inference [48,49], which has been shown to enable low-uncertainty estimates of highly correlated states measured in two pairs of mutually unbiased bases [25,50]. Our specific procedure [49] starts with a uniform (Bures) prior and uses a likelihood from the JSI measurements in the  $Z \otimes Z$  and  $X \otimes X$  bases. The estimated mean density matrices shown in Fig. 3 have fidelities  $\geq 97\%$  with respect to the ideal Bell states. Interestingly, the fidelities for  $|\Psi^\pm\rangle$  are slightly higher than those for  $|\Phi^\pm\rangle$ , which can be attributed to a combination of SPDC from residual  $\omega_{P,0}$  pump and higher accidental coincidences in the latter case. In the dual-line pump scenario, the pump frequency at  $\omega_{P,1}$  ( $\omega_{P,-1}$ ) can also populate photons in frequency bins  $I_0$  and  $S_0$  ( $I_1$  and  $S_1$ ) via down-conversion in which the matched signal or idler falls outside of the computational space. Such processes do not contribute to the ideal  $|\Phi^\pm\rangle$  state in the coincidence basis. However, in practice the presence of multipair emission means that these undesired detection events can lead to accidental coincidences; specifically, for the same rate of desired coincidences for  $|\Psi^\pm\rangle$  and  $|\Phi^\pm\rangle$ , the  $|\Phi^\pm\rangle$  cases have double the rate of single-photon detection events, leading to a four-fold increase in uncorrelated coincidences.

The impact of both imperfect carrier extinction and background processes are validated experimentally. First, for the  $\mathbb{I}_l \otimes \mathbb{I}_s$  cases in Fig. 2, the ratio of desired to undesired JSI points is around 50 for the  $|\Phi^\pm\rangle$  states, in agreement with that predicted by the 17.5 dB carrier suppression in Fig. 1(a). (For the  $|\Psi^\pm\rangle$  states where carrier



suppression is not required, the mismatched JSI points fall to the observed accidental level.)

Similarly, computing the coincidences-to-accidentals ratios (CARs) found by comparing the coincidences in Fig. 2 against their values time-shifted in the raw histograms, we obtain CARs of  $\sim 400$  for  $|\Psi^\pm\rangle$  and  $\sim 100$  for  $|\Phi^\pm\rangle$ , again matching the fourfold theoretical prediction for accidentals between the two cases. We note that the first nonideality represents a technical limitation that could be eliminated with stronger suppression of the carrier frequency (through a different EOIM or additional pump filtering). And despite the undesirable background processes for  $|\Phi^\pm\rangle$ , its practical impact is equivalent to insertion loss: whether a photon's entangled partner lies outside of the Hilbert space or is undetected due to loss, the result is an increase in uncorrelated detection events. Indeed, a simple analysis [42] reveals that the multiline scheme for  $|\Phi^\pm\rangle$  offers a higher CAR for a given correlated coincidence rate than any alternative with  $>3$  dB extra loss per photon. Considering current QFPs with discrete fiber-optic components impart about 12.5 dB loss [22], our approach for generating  $|\Phi^\pm\rangle$  is not only simpler than QFP manipulation of a  $|\Psi^\pm\rangle$  input, but also actually attains lower background in practical scenarios.

*Quantum delay sensing.*—The joint temporal correlation of time-energy entangled biphotons can be utilized for delay metrology with potential quantum advantages [27,51]. Negatively correlated entangled states (such as  $|\Psi^\pm\rangle$ ) can probe changes to the difference in the delays traversed by the photons (differential-mode delay) via nonlocal measurements only [43,52]. Entangled photons with positive frequency correlations (such as  $|\Phi^\pm\rangle$ ) can offer enhancement in delay sensitivity beyond the shot noise limit [27,53,54], by responding to changes in the sum of the signal and idler delays (common-mode delay). Combined, these complementary capabilities suggest that frequency-bin Bell states could be employed for distributed sensing applications [55,56] and monitoring delays and latencies in quantum networks. We highlight this potential using the demonstrated frequency-bin Bell states by examining their sensitivity to common-mode and differential-mode phase—fully equivalent to temporal delay through the general Fourier relationship between linear spectral phase and group delay [43,44,57]. For the special case of two-dimensional systems, *any* relative phase shift is trivially equal to a linear phase; thus any phase operation on a frequency-bin qubit can be mapped to a delay [23].

Specifically, a common-mode phase  $\varphi_c$  applied on the bins  $S_1$  and  $I_1$  results in a global phase on the  $|\Psi^\pm\rangle$  state which remains unaltered. However, the  $|\Phi^\pm\rangle$  state transforms into  $|\Phi^{(2\varphi_c)}\rangle \propto |I_0S_0\rangle + e^{2i\varphi_c}|I_1S_1\rangle$ . Such a transformation is equivalent to a common-mode delay of the form  $\tau_c = (\tau_S + \tau_I)/2 = \varphi_c \Delta\omega^{-1}$ , where  $\tau_S$  ( $\tau_I$ ) is the total delay experienced by the signal (idler) photon. That is, biphotons traveling through the same path accumulate phase

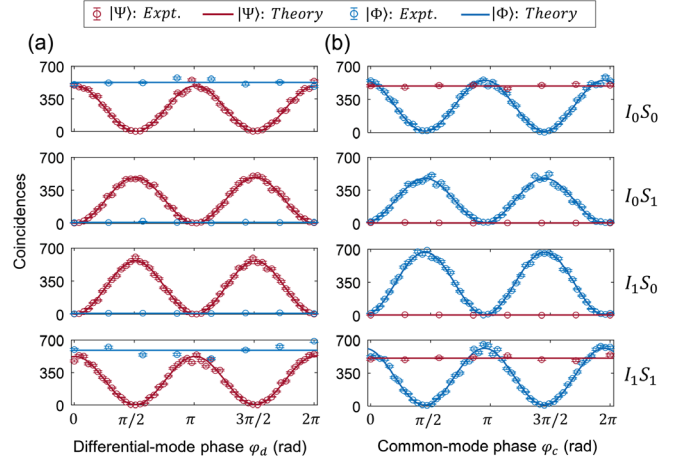


FIG. 4. Coincidence interferograms as (a) differential-mode and (b) common-mode spectral phases are scanned.

corresponding to twice the delay traversed, the origin of quantum enhancement [27]. After parallel Hadamard operations, the probability of coincidence detection between bins  $I_0$  and  $S_0$  becomes  $\mathcal{P}_{00}^{X\otimes X}(\Phi^{(2\varphi_c)}) \propto \cos^2(2\varphi_c)$  [42].

On application of differential-mode phase  $\varphi_d$  on the bins  $S_0$  and  $I_1$ , the  $|\Phi^\pm\rangle$  states are unaltered while  $|\Psi^\pm\rangle$  transforms to  $|\Psi^{(2\varphi_d)}\rangle \propto |I_0S_1\rangle + e^{2i\varphi_d}|I_1S_0\rangle$ , and the resultant coincidence probability between bins  $I_0$  and  $S_0$  after parallel Hadamard operations is  $\mathcal{P}_{00}^{X\otimes X}(\Psi^{(2\varphi_d)}) \propto \cos^2(2\varphi_d)$ . This transformation is equivalent to a differential mode delay of the form  $\tau_d = (\tau_S - \tau_I)/2 = \varphi_d \Delta\omega^{-1}$ . The coincidence probabilities for other signal-idler bin pairs after the Hadamard operation are shown in Ref. [42]. Using Shaper 1 to successively apply the common-mode phase ( $\varphi_c$  on the bins  $S_1$  and  $I_1$ ) and differential-mode phase ( $\varphi_d$  on the bins  $S_0$  and  $I_1$ ) prior to Hadamard operations, we measure coincidences between different frequency-bin pairs (plotted in Fig. 4). The experiment clearly corroborates the theoretical prediction, highlighting the capability for delay metrology using frequency-bin Bell states.

*Discussion.*—We have demonstrated generation and tomography of all four two-qubit Bell states. Readily reconfigurable between single and dual line pump conditions and relying on passive spectral filtering, our setup can synthesize any Bell state within a fixed set of four frequency bins. The capability for on-demand switching between the Bell pairs can find use in quantum cryptography applications [4,58]. Further, we demonstrate that the strong positive and negative frequency correlations in the generated Bell states can be used for sensing common-mode and differential-mode delays. By routing the signal and idler photons to different optical links, our scheme could support sensing of absolute and differential link latencies—a fundamental capability facilitated by the design's reconfigurability to produce both classes of Bell states in a single setup.

A compelling feature of frequency-bin encoding is its inherent parallelizability across many wavelength channels in a single-mode fiber. Our Bell state synthesizer is well suited to this context, as it can prepare many pairs of entangled qubits subject only to the bandwidth of SPDC and the state preparation pulse shaper. Thus, with our 5 THz-wide pulse shaper, 50 parallel Bell states could in principle be produced on the current 25 GHz-spaced grid without any additional components (modulators or pulse shapers). A wavelength-selective switch could then be used to route these states on demand to entangle many pairs of users distributed across a quantum network—perhaps supplemented with frequency-bin Bell state analyzers [26] for teleportation or entanglement swapping as well. The spectrally unentangled frequency bins required for this latter context could be realized by pulse-carving the cw pump prior to sideband generation, such that its bandwidth fills an individual bin but is less than the bin spacing; all other aspects of our method would remain unchanged.

This Letter also offers scope for analyzing related multiline pump architectures for preparing two-qubit states. While on-chip generation of generic negatively correlated two-qudit states has been investigated [59], our approach can offer further opportunities for on-chip implementation of  $|\Phi\rangle$ -like states utilizing multiline-pumped spontaneous four-wave mixing in single or series microring resonators (MRRs). In fact, through an appropriate cascade of MRR sources, it might be possible to suppress undesired biphoton generation processes such that only the signal and idler mode pairs of interest—i.e., those in the two-qubit computational basis—are efficiently produced.

We thank AdvR for loaning the PPLN ridge waveguide. A portion of this work was performed at Oak Ridge National Laboratory, operated by UT-Battelle for the U.S. Department of Energy under Contract No. DE-AC05-00OR22725. Funding was provided by the National Science Foundation (1839191-ECCS, 2034019-ECCS) and the U.S. Department of Energy, Office of Science, Advanced Scientific Computing Research, Early Career Research Program (Field Work Proposal ERKJ353).

---

\*joseph.lukens@asu.edu

- [1] K. Mattle, H. Weinfurter, P.G. Kwiat, and A. Zeilinger, *Phys. Rev. Lett.* **76**, 4656 (1996).
- [2] C. H. Bennett, G. Brassard, C. Crépeau, R. Jozsa, A. Peres, and W. K. Wootters, *Phys. Rev. Lett.* **70**, 1895 (1993).
- [3] C. Shukla, N. Alam, and A. Pathak, *Quantum Inf. Process.* **13**, 2391 (2014).
- [4] R.-H. Shi and H. Zhong, *Quantum Inf. Process.* **12**, 921 (2013).
- [5] W. Tittel, J. Brendel, H. Zbinden, and N. Gisin, *Phys. Rev. Lett.* **84**, 4737 (2000).
- [6] J.-W. Pan, D. Bouwmeester, H. Weinfurter, and A. Zeilinger, *Phys. Rev. Lett.* **80**, 3891 (1998).
- [7] A. M. Goebel, C. Wagenknecht, Q. Zhang, Y.-A. Chen, K. Chen, J. Schmiedmayer, and J.-W. Pan, *Phys. Rev. Lett.* **101**, 080403 (2008).
- [8] P.G. Kwiat, K. Mattle, H. Weinfurter, A. Zeilinger, A. V. Sergienko, and Y. Shih, *Phys. Rev. Lett.* **75**, 4337 (1995).
- [9] M. Agnew, J. Z. Salvail, J. Leach, and R. W. Boyd, *Phys. Rev. Lett.* **111**, 030402 (2013).
- [10] H.-P. Lo, T. Ikuta, N. Matsuda, T. Honjo, W. J. Munro, and H. Takesue, *Phys. Rev. Appl.* **13**, 034013 (2020).
- [11] J. Brendel, N. Gisin, W. Tittel, and H. Zbinden, *Phys. Rev. Lett.* **82**, 2594 (1999).
- [12] P. J. Shadbolt, M. R. Verde, A. Peruzzo, A. Politi, A. Laing, M. Lobino, J. C. Matthews, M. G. Thompson, and J. L. O’Brien, *Nat. Photonics* **6**, 45 (2012).
- [13] J. W. Silverstone, D. Bonneau, K. Ohira, N. Suzuki, H. Yoshida, N. Iizuka, M. Ezaki, C. M. Natarajan, M. G. Tanner, R. H. Hadfield, V. Zwiller, G. D. Marshall, J. G. Rarity, J. L. O’Brien, and M. G. Thompson, *Nat. Photonics* **8**, 104 (2014).
- [14] M. Li, Q. Zhang, Y. Chen, X. Ren, Q. Gong, and Y. Li, *Micromachines* **11**, 1111 (2020).
- [15] B. Brecht, D. V. Reddy, C. Silberhorn, and M. G. Raymer, *Phys. Rev. X* **5**, 041017 (2015).
- [16] P. Manurkar, N. Jain, M. Silver, Y.-P. Huang, C. Langrock, M. M. Fejer, P. Kumar, and G. S. Kanter, *Optica* **3**, 1300 (2016).
- [17] V. Ansari, J. M. Donohue, B. Brecht, and C. Silberhorn, *Optica* **5**, 534 (2018).
- [18] F. Graffitti, P. Barrow, A. Pickston, A. M. Brańczyk, and A. Fedrizzi, *Phys. Rev. Lett.* **124**, 053603 (2020).
- [19] S. Merkouché, V. Thiel, A. O. C. Davis, and B. J. Smith, *Phys. Rev. Lett.* **128**, 063602 (2022).
- [20] M. Kues, C. Reimer, J. M. Lukens, W. J. Munro, A. M. Weiner, D. J. Moss, and R. Morandotti, *Nat. Photonics* **13**, 170 (2019).
- [21] P. Imany, J. A. Jaramillo-Villegas, O. D. Odele, K. Han, D. E. Leaird, J. M. Lukens, P. Lougovski, M. Qi, and A. M. Weiner, *Opt. Express* **26**, 1825 (2018).
- [22] H.-H. Lu, J. M. Lukens, N. A. Peters, O. D. Odele, D. E. Leaird, A. M. Weiner, and P. Lougovski, *Phys. Rev. Lett.* **120**, 030502 (2018).
- [23] H.-H. Lu, E. M. Simmerman, P. Lougovski, A. M. Weiner, and J. M. Lukens, *Phys. Rev. Lett.* **125**, 120503 (2020).
- [24] L. Zhang, C. Cui, J. Yan, Y. Guo, J. Wang, and L. Fan, *arXiv:2111.12784*.
- [25] H.-H. Lu, J. M. Lukens, N. A. Peters, B. P. Williams, A. M. Weiner, and P. Lougovski, *Optica* **5**, 1455 (2018).
- [26] N. B. Lingaraju, H.-H. Lu, D. E. Leaird, S. Estrella, J. M. Lukens, and A. M. Weiner, *Optica* **9**, 280 (2022).
- [27] V. Giovannetti, S. Lloyd, and L. Maccone, *Phys. Rev. A* **65**, 022309 (2002).
- [28] V. Giovannetti, S. Lloyd, and L. Maccone, *Nature (London)* **412**, 417 (2001).
- [29] In this context, “narrow band” implies that the individual bin widths are smaller than all other characteristic frequency scales in the problem—e.g., variations in the phase-matching function, pulse shaper filter widths, or dispersion.
- [30] W. P. Grice and I. A. Walmsley, *Phys. Rev. A* **56**, 1627 (1997).
- [31] D. S. Hum and M. M. Fejer, *C.R. Phys.* **8**, 180 (2007).

- [32] S. E. Harris, *Phys. Rev. Lett.* **98**, 063602 (2007).
- [33] M. B. Nasr, S. Carrasco, B. E. A. Saleh, A. V. Sergienko, M. C. Teich, J. P. Torres, L. Torner, D. S. Hum, and M. M. Fejer, *Phys. Rev. Lett.* **100**, 183601 (2008).
- [34] S. Sensarn, G. Y. Yin, and S. E. Harris, *Phys. Rev. Lett.* **104**, 253602 (2010).
- [35] O. D. Odele, J. M. Lukens, J. A. Jaramillo-Villegas, C. Langrock, M. M. Fejer, D. E. Leaird, and A. M. Weiner, *Opt. Express* **23**, 21857 (2015).
- [36] O. D. Odele, J. M. Lukens, J. A. Jaramillo-Villegas, P. Imany, C. Langrock, M. M. Fejer, D. E. Leaird, and A. M. Weiner, *APL Photonics* **2**, 011301 (2017).
- [37] A. M. Brańczyk, A. Fedrizzi, T. M. Stace, T. C. Ralph, and A. G. White, *Opt. Express* **19**, 55 (2011).
- [38] P. B. Dixon, J. H. Shapiro, and F. N. C. Wong, *Opt. Express* **21**, 5879 (2013).
- [39] C. Chen, C. Bo, M. Y. Niu, F. Xu, Z. Zhang, J. H. Shapiro, and F. N. C. Wong, *Opt. Express* **25**, 7300 (2017).
- [40] This analysis also holds for spontaneous four-wave mixing (SFWM), with the single  $\alpha$  terms replaced by sums of products of pump amplitudes. Processes with identical total biphoton energy will still depend on the same pump contributions, so that SFWM will face the same general limits to arbitrary state production as SPDC.
- [41] P. Imany, O. D. Odele, M. S. Alshaykh, H.-H. Lu, D. E. Leaird, and A. M. Weiner, *Opt. Lett.* **43**, 2760 (2018).
- [42] See Supplemental Material at <http://link.aps.org/supplemental/10.1103/PhysRevLett.129.230505>, which includes Refs. [22,25,43–45], for a performance comparison with the QFP, derivation of coincidence probabilities as functions of temporal delay, and details on experimental components.
- [43] S. Seshadri, N. Lingaraju, H.-H. Lu, P. Imany, D. E. Leaird, and A. M. Weiner, [arXiv:2202.11816](https://arxiv.org/abs/2202.11816).
- [44] A. Pe'er, B. Dayan, A. A. Friesem, and Y. Silberberg, *Phys. Rev. Lett.* **94**, 073601 (2005).
- [45] B. J. Pearson and D. P. Jackson, *Am. J. Phys.* **78**, 471 (2010).
- [46] A. Monmayrant and B. Chatel, *Rev. Sci. Instrum.* **75**, 2668 (2004).
- [47] J. T. Willits, A. M. Weiner, and S. T. Cundiff, *Opt. Express* **20**, 3110 (2012).
- [48] J. M. Lukens, K. J. Law, A. Jasra, and P. Lougovski, *New J. Phys.* **22**, 063038 (2020).
- [49] H.-H. Lu, K. V. Myilswamy, R. S. Bennink, S. Seshadri, M. S. Alshaykh, J. Liu, T. J. Kippenberg, D. E. Leaird, A. M. Weiner, and J. M. Lukens, *Nat. Commun.* **13**, 4338 (2022).
- [50] H.-H. Lu, N. B. Lingaraju, D. E. Leaird, A. M. Weiner, and J. M. Lukens, *Opt. Express* **30**, 10126 (2022).
- [51] V. Giovannetti, S. Lloyd, and L. Maccone, *Science* **306**, 1330 (2004).
- [52] R. Quan, R. Dong, X. Xiang, B. Li, T. Liu, and S. Zhang, *Rev. Sci. Instrum.* **91**, 123109 (2020).
- [53] O. Kuzucu, M. Fiorentino, M. A. Albota, F. N. C. Wong, and F. X. Kärtner, *Phys. Rev. Lett.* **94**, 083601 (2005).
- [54] O. Kuzucu, F. N. C. Wong, S. Kurimura, and S. Tovstonog, *Phys. Rev. Lett.* **101**, 153602 (2008).
- [55] S.-R. Zhao, Y.-Z. Zhang, W.-Z. Liu, J.-Y. Guan, W. Zhang, C.-L. Li, B. Bai, M.-H. Li, Y. Liu, L. You, J. Zhang, J. Fan, F. Xu, Q. Zhang, and J.-W. Pan, *Phys. Rev. X* **11**, 031009 (2021).
- [56] V. Giovannetti, S. Lloyd, and L. Maccone, *Nat. Photonics* **5**, 222 (2011).
- [57] A. M. Weiner, *Ultrafast Optics* (Wiley, New York, 2009).
- [58] L. Chun-Yan, Z. Hong-Yu, W. Yan, and D. Fu-Guo, *Chin. Phys. Lett.* **22**, 1049 (2005).
- [59] M. Liscidini and J. Sipe, *Opt. Lett.* **44**, 2625 (2019).